Available online at www.sciencedirect.com
ScienceDirect
Electrochemistry Communications 9 (2007) 1907–1912
electrochemistry communications
www.elsevier.com/locate/elecom

Microstructure changes to iron nanoparticles during discharge/charge cycles

Kuo-Cheng Huang, Kan-Sen Chou *

Department of Chemical Engineering, National Tsing-Hua University, 101, Section 2, Kuang-Fu Road, Hsinchu 30013, Taiwan

Received 7 March 2007; received in revised form 25 April 2007; accepted 4 May 2007
Available online 17 May 2007

Abstract

Iron nanoparticles that were synthesized by chemical reduction were used as the active material at the electrode, followed by measurement of their capacity during discharge/charge cycles. The discharge capacity of the first cycle was extremely high, 510 mAh/g-Fe, at a current density of 200 mA/g-Fe, indicating a marked increase in the capacity and the output current of iron electrodes when nanoparticles of iron, instead of micron-sized particles were used as the active materials. However, this capacity deteriorated rapidly during the discharge/charge cycles, while the size of iron nanoparticles increased, suggesting that the dissolution and re-crystallization of iron could have occurred during these cycles. A good correlation was found between the capacities and the surface areas of iron nanoparticles following each cycle. Our result further demonstrated that the capacity depends only on the surface area of iron particles, varying by 30 mAh with every 1 m^2 of iron.

Keywords: Iron nanoparticle; Iron electrode; Nickel–iron battery

1. Introduction

Developed in the 1900s, nickel–iron battery has the merits of low cost, a long life cycle, safety of use, and environmental friendliness. For safety and environmental reasons, the nickel–iron battery is a promising alternative energy source for electric vehicles. A nickel–iron battery comprises nickel oxyhydroxide (NiOOH) as the cathode and metallic iron as the anode. The theoretical capacity for the two electron oxidation of the iron electrode is as high as 962 mAh/g-Fe. However, traditional iron electrodes only have a capacity of lower than 350 mAh/g-Fe, which fact is a critical problem in commercial applications of Ni–Fe batteries.

Improving the utilization of iron particles is of priority concern when attempting to increase the capacity of iron electrodes. Iron electrodes made by sintering typically have a higher capacity than those make by pressing iron particles, because they have greater porosity, and consequently greater contacts between the iron particles to the electrolyte. Passivation of the iron particle surface is another problem in limiting the capacity of iron electrodes. Therefore, sulfide additives are usually added to activate the particle surfaces in iron electrodes [1–5]. Yet, even after these treatments, the utilization of iron particles remained under 30%. Restated, only a thin layer of iron on the particle surface can be used. Table 1 briefly summarizes the literature on iron electrodes.

As discussed above, the utilization of iron particles is restricted only to a small portion of its surface atoms. An increase in capacity is expected when nanoparticles of iron are used instead of micron-sized particles. Therefore, this work examines the feasibility of such a concept and reports on the true performance of such an electrode that is made from nanosized iron particles.

* Corresponding author. Tel.: +886 35 713691; fax: +886 35 715408.
E-mail address: kschou@che.nthu.edu.tw (K.-S. Chou).

1388-2481/$ - see front matter © 2007 Elsevier B.V. All rights reserved.
doi:10.1016/j.elecom.2007.05.001

Table 1
Summary of properties of iron electrodes

Electrode type	Additive	Maximum capacity (mAh/g-Fe)	Output current (mA/g-Fe)	Reference
Pressed	FeS	175	12.5	Caldas et al. [4]
Pressed (porous)	FeS	310	12.5	Caldas et al. [4]
Pressed	PbS	310	12.9	Souza et al. [5]
Sintered	None	339	18	Tong et al. [13]

2. Experimental

2.1. Synthesis of iron nanoparticles

Iron nanoparticles were synthesized by mixing the precursor solution with a reducing agent solution. The precursor solution was made of 4.0 g of ferric chloride ($FeCl_3$, 97%, Showa, Japan) in 50 ml of de-ionized water. 6.0 g of sodium borohydride ($NaBH_4$, 98%, Lancaster, England) was dissolved in 100 ml of de-ionized water to make the reducing agent solution. The reducing agent solution was immersed in the ice-bath before the precursor solution was added dropwise at a rate of 0.13 ml/s using the micro-tube pump (MP-3N, EYELA, Japan). The synthesis reaction was considered complete when bubbles were not longer generated. The product, black powder, was recovered using a strong magnet. The powder was washed twice using hot water and once using cold water to remove the residual by-product.

2.2. Fabrication and electrochemical measurement of iron nanoparticle electrode

A nickel–iron cell system was established to measure the discharge capacity of an iron nanoparticle electrode. The nickel electrode was overdosed so that the cell performance was limited by the iron nanoparticle electrode. The capacity of nickel electrode was about 2000 mAh, which was four times that of the iron electrode. Following the washing process, fresh iron nanoparticles were rapidly stuffed manually into the nickel foam (ShenYang Golden Champower New Material, China) to make an iron nanoparticle electrode. The nickel foam (porosity = 97%, pore size = 110 ppi), 84 mm × 42 mm × 1.8 mm in size, was used not only to hold iron nanoparticles but also to collect discharged current. The mass of the iron nanoparticles in the electrode was 1.3 g, as determined from the stoichiometric calculation of one batch synthesis with 100% conversion of iron precursor. The electrolyte comprises 8 M NaOH and 1 M LiOH.

The discharge/charge cycle test for the nickel–iron cell was performed using a battery testing system (AcuTech BAT-760, Taiwan) at room temperature. The cutoff voltage was set to 1000 mV.

The cyclic voltammetry was performed using iron nanoparticle electrode as the working electrode, nickel oxyhydroxide electrode as the counter electrode, and Ag/AgCl electrode as the reference electrode. The electrolyte was 8 M KOH solution. The scan rate was 0.5 mV/s and the scan range was from −1.6 V to −0.2 V.

2.3. Iron nanoparticle analysis following discharge/charge cycles

Since performing an in situ analysis of the microstructure of iron nanoparticles during capacity measurement is impossible, iron electrodes must be disassembled after various cycles to collect samples for analysis. After a certain discharge/charge cycle, the iron nanoparticle electrode was immersed in de-ionized water and then ultrasonicated to separate the iron nanoparticles from the nickel foam. The iron nanoparticles were washed using de-ionized water for three times and then using acetone another three times. The iron nanoparticles were dried at room temperature for further analysis.

2.4. Characterization

The morphology of iron nanoparticles was observed by the scanning electron microscope (SEM; S-4700, Hitachi, Japan). X-ray diffraction (XRD; UD-3000, Scintag, USA) was performed to determine the crystal structure of iron nanoparticles. The specific surface area of iron nanoparticles was determined using the Brunauer–Emmet–Teller (BET) method (ASAP 2000, Micrometrics, USA).

3. Results and discussion

3.1. Synthesis of iron nanoparticles

Fig. 1a presents the morphology of synthesized iron nanoparticles. Most of the primary particles have diameters of between 30 and 70 nm, but they are connected in chains because of the slight magnetic attraction among them. Similar results have been presented elsewhere [6–8]. The specific surface area (BET) of these iron nanoparticles was 25.3 m^2/g, which approximately corresponds to the sizes from microscopy observation. The XRD analysis shown in Fig. 1b indicates that the nanoparticles are almost amorphous with a very weak characteristic peak of α-phase iron, suggesting the metallic nature of the nanoparticles. This result agrees closely with those elsewhere [8,9].

3.2. Discharge properties of iron nanoparticles

As shown in Fig. 2a, the iron nanoparticles exhibited a remarkable discharge capacity of 510 mAh/g-Fe during the first discharge at a high current density of 200 mA/g-Fe. When iron nanoparticles were the active materials,

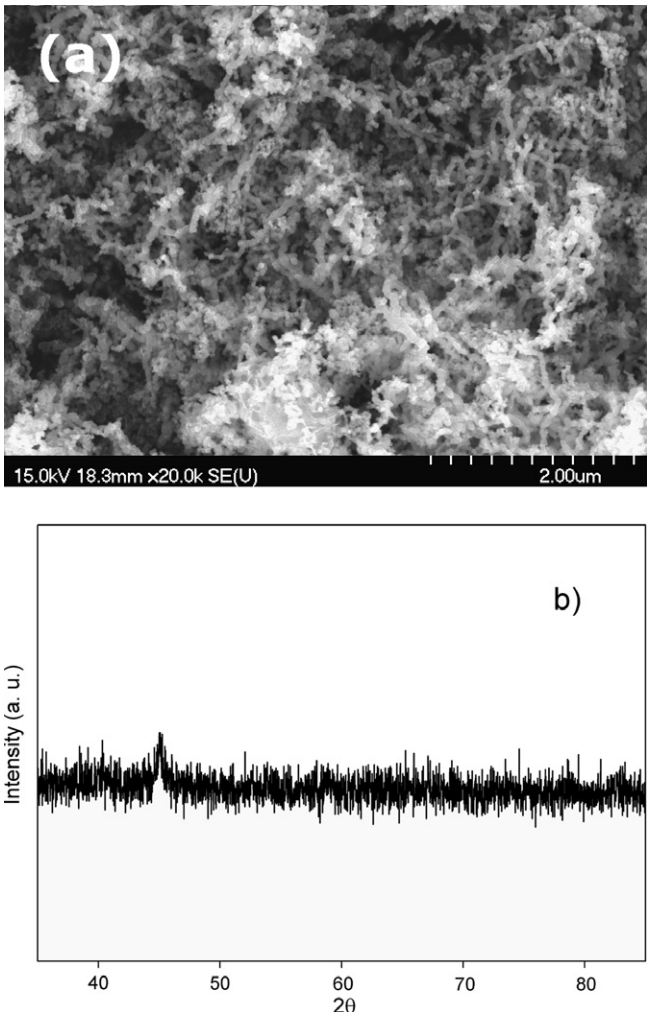

Fig. 1. (a) SEM picture of iron nanoparticles, magnification = 20,000× and (b) XRD pattern of iron nanoparticles.

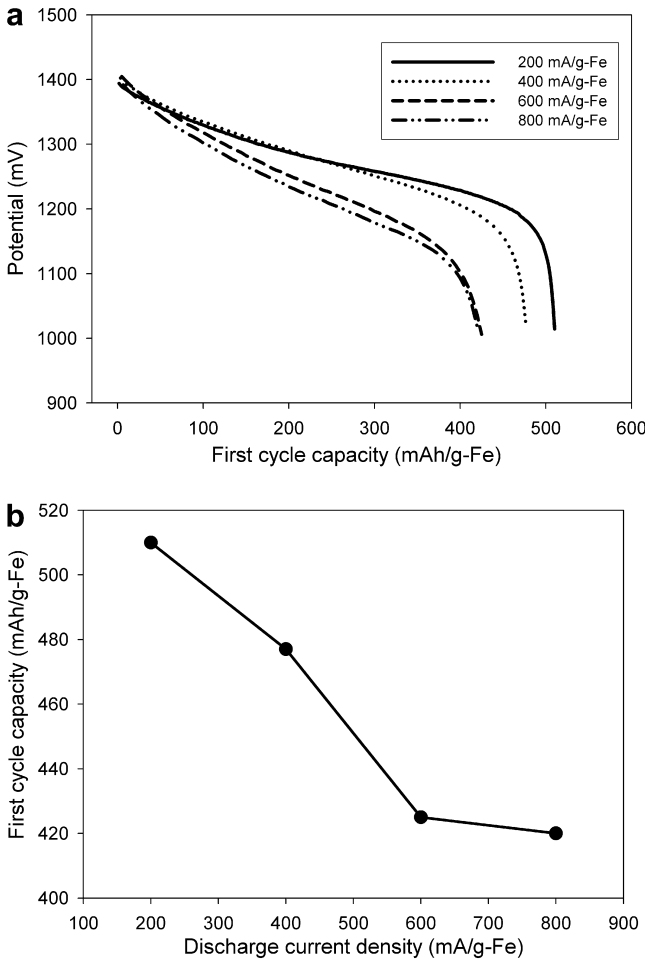

Fig. 2. (a) Typical discharge curve of iron nanoparticle electrodes and (b) first cycle capacity of iron nanoparticle at various discharge current densities.

the capacity was significantly higher than that of the traditional iron electrodes that are referred in Table 1. This increase in capacity can be mainly attributed to the large surface area of iron nanoparticles, because no additive was used. A higher capacity is expected when additives are included. Related work is underway.

Another possible explanation for the high capacity of iron nanoparticle electrode is the large porosity of the iron nanoparticle electrode. Since the iron nanoparticles were connected in chains, the high aspect ratio of this structure enables more contacts to be made between iron nanoparticles and electrolyte, improving the capacity of iron nanoparticle electrodes.

The output current density of the iron nanoparticle electrode markedly exceeded that of the traditional iron electrode. As shown in Fig. 2b, the iron nanoparticle electrode retained a capacity of 420 mAh/g-Fe, even when the discharge current density was increased to 800 mA/g-Fe. In comparison, the capacity of the traditional pressed iron electrode without an additive decreased from 125 mAh/g-Fe to 45 mAh/g-Fe as the discharge current increased from 12.5 mA/g-Fe to 57.5 mA/g-Fe [4].

3.3. Cyclic voltammetry of iron nanoparticle electrode

Cyclic voltammogram of iron nanoparticle during the first cycle shown in Fig. 3 presents two pairs of reduction/oxidation peaks as Red_1/Ox_1 and Red_2/Ox_2 at -1.31 V/-0.88 V and -1.10 V/-0.77 V versus Ag/AgCl, respectively. The Red_1 peak was almost not noticeable because it was probably superposed on the current for the hydrogen evolution reaction. By comparison to pure iron particles [4,10], the first reduction/oxidation peaks are attributed to the reaction of Fe to $Fe(OH)_2$, while the second reduction/oxidation peaks is attributed to the reaction of $Fe(OH)_2$ to Fe(III).

3.4. Deterioration of capacity of iron nanoparticle electrode

Although the iron nanoparticle electrode had an outstanding discharge capacity during the first cycle, the recycling property of this electrode was relatively poor. Very different from the traditional iron electrodes, the iron nanoparticle electrode deteriorated rapidly after the discharge/charge cycles, as shown in Fig. 4. The capacity

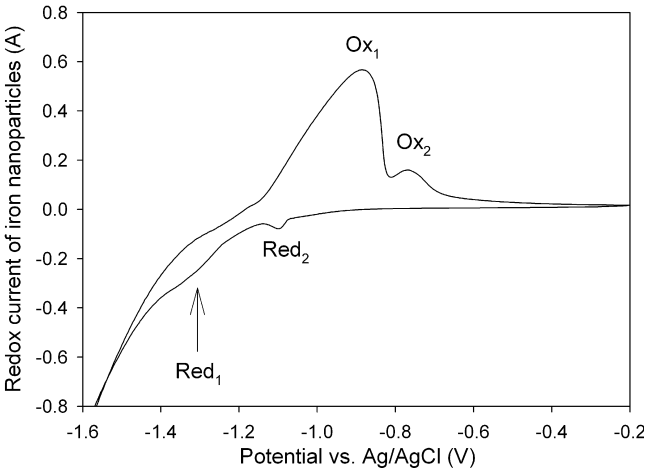

Fig. 3. Cyclic voltammogram of iron nanoparticles.

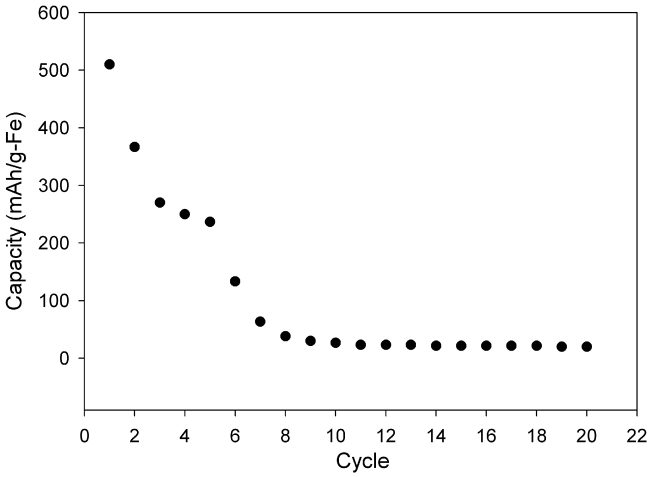

Fig. 4. Deterioration of capacity of iron nanoparticle electrode.

reached its maximum in the first discharge cycle and declined rapidly to minimum after about 10 cycles. The decrease in the capacity accompanied corresponding changes in the microstructure of the iron nanoparticles in the electrode, as shown in Fig. 5. The microscopic observations revealed that the iron nanoparticles gradually grew with the discharge/charge cycles. These images implied that the iron nanoparticles could dissolve to form

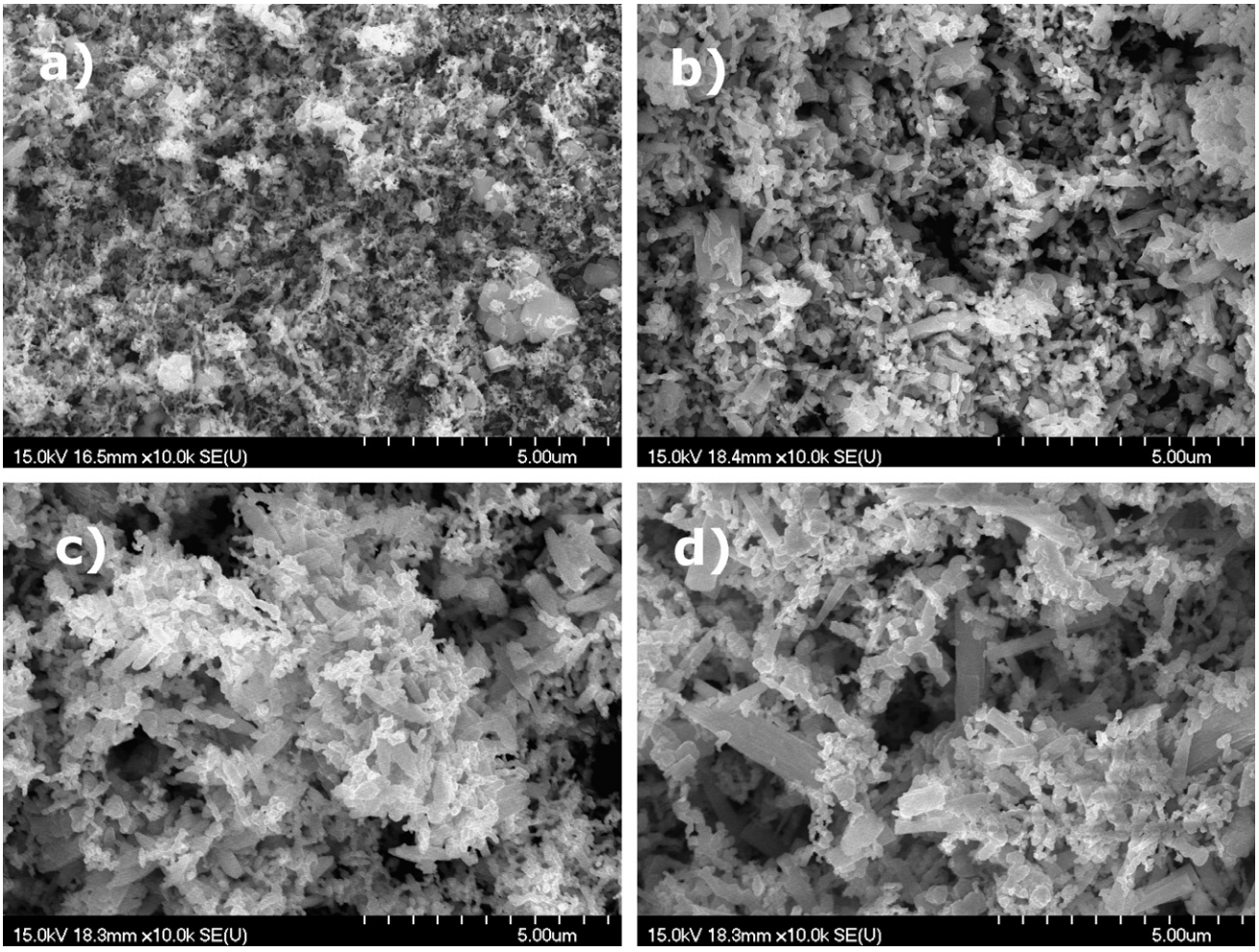

Fig. 5. SEM pictures of iron nanoparticles after various numbers discharge/charge cycles and then charged, (a) 1 cycle, (b) 5 cycles, (c) 10 cycles and (d) 20 cycles.

the ferrite ($HFeO_2^-$) intermediate during the discharge process and then re-crystallize during the charge process [11,12]. Subsequently, the nanoparticles grew to minimize the surface energy and achieve a thermodynamically stable system.

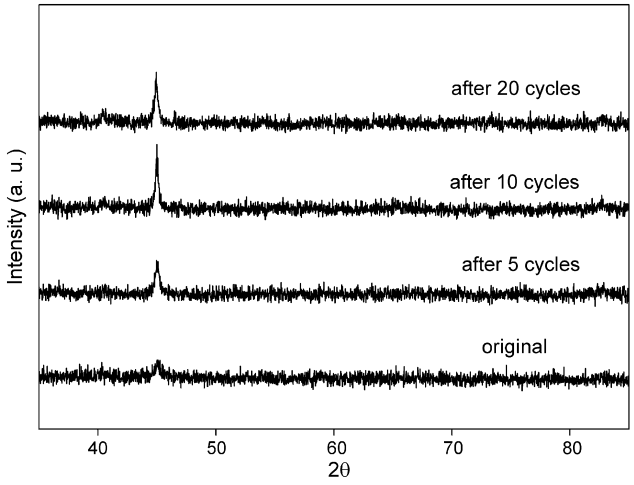

Fig. 6. XRD patterns of iron nanoparticles after various numbers of discharge/charge cycles.

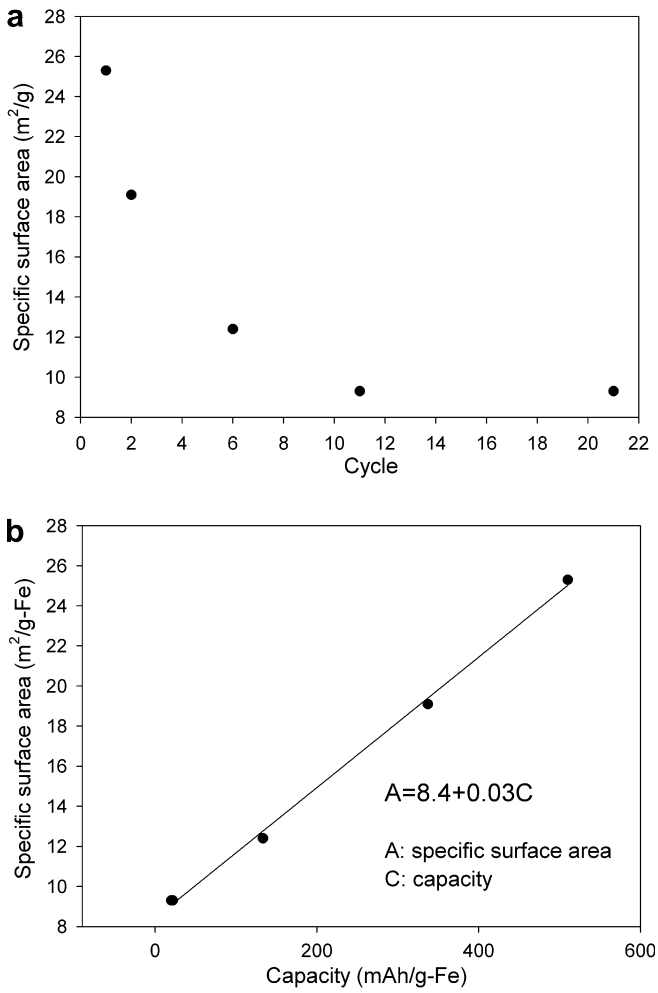

Fig. 7. (a) Specific surface area of iron nanoparticles versus discharge/charge cycles and (b) correlation between surface area and capacity.

X-ray diffraction was performed next on the iron nanoparticles following various numbers of discharge/charge cycles. The results are plotted in Fig. 6. The pattern indicated that the characteristic peak of iron gradually grew after several cycles. This result is consistent with the microscopic observations, presented in Fig. 5, indicating that the re-crystallization improves the crystalline structure of iron particles.

3.5. Correlation between capacity and specific surface area of iron nanoparticles

Fig. 7a presents the specific surface area of iron nanoparticles following various numbers of discharge/charge cycles. Fig. 7b plots the correlation between the specific surface area and the discharge capacity. A good linear relationship existed between these two sets of numbers, indicating that the capacity of iron nanoparticle electrode was linearly proportional to the surface area of iron nanoparticles. The slope obtained from the fitting suggested that a specific surface area of 1 m^2/g-Fe contributed to a discharge capacity of 30 mAh/g-Fe at a discharge current density of 200 mA/g-Fe when no activating additive was added.

The intercept indicated a specific surface area of 8.4 m^2/g-Fe, which was about 1/3 that of iron nanoparticles, not reacting during the process. This result may have followed from the poor conductive network of iron nanoparticles, since these particles were not subjected to any sintering before measurement.

4. Conclusions

Iron nanoparticles without any additive were demonstrated to have a high discharge capacity at high current density, because of their large specific surface area. However, this high capacity declines quickly with the number of cycles, because the nanoparticles grow by dissolution and re-crystallization. A linear correlation was established between capacity and specific surface area, showing 30 mAh/g-Fe for 1 m^2/g-Fe of iron particles. More work is required to find ways to inhibit or to slow the growth of these iron nanoparticles to improve the recycling performance.

Acknowledgement

The authors thank the National Science Council of the Republic of China, Taiwan, for financially supporting this research under Contract No. NSC 95-2214 – E007 – 236.

References

[1] K. Vijayamohanan, A.K. Shukla, S. Sathyanarayana, Journal of Electroanalytical Chemistry and Interfacial Electrochemistry 289 (1990) 55.
[2] T.S. Balasubramanian, A.K. Shukla, J. Power Sources 41 (1993) 99.

[3] P. Periasamy, B.R. Babu, S.V. Iyer, J. Power Sources 62 (1996) 9.
[4] C.A. Caldas, M.C. Lopes, I.A. Carlos, J. Power Sources 74 (1998) 108.
[5] C.A.C. Souza, I.A. Carlos, M. Lopes, G.A. Finazzi, M.R.H. De Almeida, J. Power Sources 132 (2004) 288.
[6] K.C. Huang, S.H. Ehrman, Langmuir 23 (2007) 1419.
[7] L. Zhang, A. Manthiram, IEEE Trans. Magn. 32 (1996) 4481.
[8] C.Y. Wang, Z.Y. Chen, B. Cheng, Y.R. Zhu, H.J. Liu, Materials Science and Engineering B: Solid-State Materials for Advanced Technology 60 (1999) 223.
[9] G.N. Glavee, K.J. Klabunde, C.M. Sorensen, G.C. Hadjipanayis, Inorg. Chem. 34 (1995) 28.
[10] K. Ujimine, A. Tsutsumi, J. Power Sources 160 (2006) 1431.
[11] C. Chakkaravarthy, P. Periasamy, S. Jegannathan, K.I. Vasu, J. Power Sources 35 (1991) 21.
[12] A.K. Shukla, M.K. Ravikumar, T.S. Balasubramanian, J. Power Sources 51 (1994) 29.
[13] C.S. Tong, S.D. Wang, Y.Y. Wang, C.C. Wan, J. Electrochem. Soc. 129 (1982) 1173.